

1 **Carbon emission reduction requires attention to the contribution of natural gas use:**
2 **Combustion and leakage**

3 Haoyuan Chen^{1,5}, Tao Song^{1,5*}, Xiaodong Chen², Yinghong Wang¹, Mengtian Cheng¹, Kai
4 Wang¹, Fuxin Liu⁴, Baoxian Liu³, Guiqian Tang^{1,5*}, Yuesi Wang^{1,5}

5 Correspondence to Guiqian Tang (tgq@dq.cern.ac.cn) Tao Song (st@dq.cern.ac.cn)

6 1. Key Laboratory of Atmospheric Environment and Extreme Meteorology, Institute of
7 Atmospheric Physics, Chinese Academy of Sciences, Beijing, China

8 2. Beijing Aozuo Ecological Instrument Co., Ltd., Beijing 100080, China

9 3. Beijing Key Laboratory of Airborne Particulate Matter Monitoring Technology, Beijing
10 Municipal Environmental Monitoring Center, Beijing, 100048, China

11 4. Anhui University of Science and Technology, Anhui 232001, China

12 5. University of Chinese Academy of Sciences, Beijing 100049, China

13 Abstract: Natural gas will continue to replace coal in the process of global energy structure reform,
14 but its leakage potential can delay the realization of global carbon neutrality. To quantify its impact,
15 we established a carbon dioxide (CO₂) and methane (CH₄) flux detection platform on the 220-m
16 platform of the Institute of Atmospheric Physics, Chinese Academy of Sciences, located in
17 northwestern Beijing. The observation results indicated that the daily mean CO₂ and CH₄ fluxes
18 were $12.21 \pm 1.75 \text{ } \mu\text{mol} \cdot \text{m}^{-2} \cdot \text{s}^{-1}$ and $95.54 \pm 18.92 \text{ } \text{nmol} \cdot \text{m}^{-2} \cdot \text{s}^{-1}$, respectively. The fluxes were
19 significantly correlated with natural gas consumption, indicating that natural gas has become a
20 common source of CH₄ and CO₂, the combustion of which releases CO₂, while its leakage processes
21 emit CH₄. Vehicle-based identification demonstrated that CH₄ can escape at the production, storage
22 and use stages of natural gas. Based on natural gas consumption data, the upper limit of the
23 calculated natural gas leakage rate in Beijing reached $1.12\% \pm 0.22\%$, indicating that the
24 contribution of CH₄ to climate change could reach 23 % of that of CO₂ on a 20-year scale. Natural
25 gas leakage was estimated to delay the time for China to achieve carbon neutrality by at least almost
26 four years.

27 **KEY WORDS:**

28 CO₂ flux, CH₄ flux, Eddy covariance, Natural gas leakage, Climate forcing, Carbon neutrality

29 **1. INTRODUCTION**

30 In 2015, the 1.5 °C temperature control target was proposed in the Paris Agreement to reduce

31 the occurrence of extreme weather events(Seneviratne et al., 2018). To achieve this goal, it is
32 necessary to actively promote the low-carbon development transformation of the economic system,
33 especially energy transformation. In this process, natural gas plays an important role, and typical
34 countries have indicated a trend of coal reduction and gas increase during energy structure
35 adjustment over the past century. It is expected that global natural gas consumption will continue to
36 increase by 2035.

37 Natural gas is commonly referred to as a clean alternative to coal, but its main component is
38 methane, with a global warming potential (GWP) that is 29.8 times greater than that of carbon
39 dioxide at the hundred-year scale(Environmental-Protection-Agency, 2024). If 3.4 % of methane
40 leaks into the atmosphere before natural gas combustion, the advantages of natural gas over coal
41 will become negligible(Kemfert et al., 2022). Recent studies have suggested that the average loss
42 rate of natural gas in cities worldwide ranges from 3.3 % to 4.7 %(Sargent et al., 2021). According
43 to statistics from the International Energy Agency (www.iea.org) in 2020, methane leakage in the
44 global oil and gas industry reached 72 million tons and amounted to 6 billion tons of carbon dioxide
45 equivalent (CO₂e) within 20 years. Therefore, it is unclear whether natural gas can become a
46 bridging material for energy transformation.

47 One important prerequisite is to determine the contribution of natural gas leakage during coal-
48 to-gas conversion to urban methane (CH₄) emissions and its climate effects. At present, conventional
49 CH₄ monitoring methods include ground, aviation, and satellite monitoring methods. Ground
50 monitoring aims to detect the atmospheric CH₄ concentration through the installation of sensors and
51 monitoring stations at fixed locations or on vehicles(Wunch et al., 2016). Notably, monitoring
52 equipment is often installed near potential emission sources, with high detection accuracy but
53 generally a limited spatial range. The aviation monitoring method can be employed to identify large-
54 scale CH₄ emissions through measurement techniques such as drones or aircraft but cannot be used
55 to achieve long-term monitoring(Duren et al., 2019; Frankenberg et al., 2016; Sherwin et al., 2024).
56 Satellite methods can compensate for the shortcomings of the former two methods(Chen et al., 2022;
57 Cusworth et al., 2018; Shen et al., 2023), which exhibit interference from clouds and require
58 significant labor and financial investments.

59 The eddy covariance method, which is based on tall towers, enables long-term monitoring of

60 methane emissions, thus facilitating the identification of methane sources in specific areas. However,
61 it should be noted that this method has certain limitations during urban flux measurements at higher
62 altitudes, as larger air volumes in the measurement system may lead to a significant imbalance
63 between the observed vertical turbulence exchange and surface net flux compared with those at
64 typical measurement heights. However, this deficiency should be considered in conjunction with
65 the advantages of urban tower measurements because cities typically correspond to deeper rough
66 sublayers that can extend to 2–5 times the average building height(Barlow, 2014). Therefore,
67 increasing the measurement altitude can help characterize the turbulent exchange between this layer
68 and the inertial sublayer.

69 Developing countries are the main driving force behind the continuous growth in global energy
70 demand. As Beijing is the capital of the world's largest developing country and the first city within
71 China to complete the coal-to-gas conversion process, clarifying the natural gas leakage process in
72 Beijing can provide guidance for energy transformation in developing countries regionally and even
73 globally. In this study, three aspects related to natural gas were investigated as follows. First, the
74 fluxes of CH₄ and CO₂ were observed simultaneously via the eddy covariance method, which was
75 used to investigate the impact of the coal-to-gas policy on CO₂ and CH₄ in Beijing, including the
76 magnitude of CO₂ emission and the common effects on the sources of both. Second, with navigation
77 experiments, the natural gas leakage process in Beijing has been confirmed, and the emission levels
78 of natural gas at different stages have been further roughly estimated, which provides certain
79 effective insights for the control of natural gas leakage in Beijing. Third, we discuss climate forcing
80 caused by natural gas leakage while considering the CO₂ flux as a basis, calculate the natural gas
81 leakage rate with statistical data, and estimate the impact of natural gas leakage on China's carbon
82 peak and carbon neutrality in conjunction with existing reports.

83

84 **2. METHODS**

85 **2.1 Instrument setup for eddy covariance measurement**

86 The measurements were conducted at a 325-m high meteorological tower in northwestern
87 Beijing, with a closed-path observation system installed on a platform at a height of 220 m, which
88 included a dual laser gas analyzer (QC-TILDAS-DUAL, Aerodyne Research Inc., USA), three-

dimensional ultrasonic anemometer (Gill Instruments, Ltd., Lymington, Hampshire, UK), vacuum pump (XDS35i, BOC Edwards, UK), data collector (CR6, Campbell Scientific Inc., USA), and other accessories. In the dual laser gas analyzer, tunable infrared laser direct absorption spectroscopy (TILDAS) technology is used to detect the most significant fingerprint transition frequencies of molecules within the mid-infrared wavelength range. The analyzer has an optical path of up to 76 m and can measure H₂O, CO₂ and CH₄ simultaneously. Similar instruments have been applied to observe outdoor ecosystems (Zöll et al., 2016). Under the action of a vacuum pump, the air sample enters the instrument room at a flow rate of 2 lpm through a polytetrafluoroethylene sampling tube with a length of 3 m and an inner diameter of 3 mm (Figure S1). Instrument calibration includes zero-point and range calibration processes. High-purity nitrogen gas (>99.999%) was used for zero-point calibration at 1-hour intervals. In this process, the corresponding solenoid valve was opened, which was automatically controlled by TDLWintel software, and range calibration was performed at the factory. In addition, before the experiment, we calibrated the gas analyzer using CO₂ (401 ppm) and CH₄ (2190 ppb) standard gases. We found that the measured and standard gas concentrations differed by less than 1%, indicating satisfactory instrument performance. Therefore, we did not perform range calibration later. The instrument was placed in an insulated box equipped with air conditioning to ensure normal operation of the laser. Both instruments were operated at a sampling frequency of 10 Hz. The data collector and high-frequency instrument were timed according to the network and global positioning system (GPS), respectively, to maintain synchronization. To minimize the twisting effect of the flux tower on the incoming air, a three-dimensional ultrasonic anemometer was installed at the end of a 1.5-m long support arm facing southeast China in summer. This measurement lasted from June 11 to September 7, 2022, during which the nitrogen cylinder was replaced, and the instrument was debugged on June 18 and 19. From July 12 to 26, the experiment was stopped due to failure of the tower power supply.

2.2 Flux data processing

The flux data processing operation in this study is based on the eddy covariance technique via EddyPro software (version 6.2.1, Li COR, Inc.; Lincoln, Nebraska, USA). An average flux calculation period of 30 minutes was selected (Lee, 2004). Before calculating half-hourly fluxes, spike detection and data rejection algorithms were applied like follows as described by Vickers et

118 al., (1997): Take a moving window with a width equal to 1/6 of the averaging period (typically 5
119 minutes) and calculate the mean and standard deviation of the time series within the window. Define
120 outliers as any data points deviating from the mean by n times the standard deviation (initial n =
121 3.5). Replace the identified outliers with linearly interpolated values from adjacent points.
122 Consecutive outliers ≤ 3 are treated as a single outlier; consecutive outliers ≥ 4 are considered local
123 trends and excluded from outlier classification. Iteratively increase n by 0.1 per cycle until no
124 outliers are detected or 20 iterations are reached. Advance the window by half its width (step size)
125 and repeat outlier detection/removal for the next window. Continue this process until all outliers are
126 processed within the averaging period. If outliers exceed 1 % of the total data points in any averaging
127 period, discard that entire period.

128 The double rotation method proposed by Kaimal et al., (1994) was employed for tilt correction.
129 The delay time caused by the spatial separation of gas analyzers and three-dimensional ultrasonic
130 anemometers (as well as the injection pipeline of closed-path systems) was corrected via the
131 maximum covariance method(Fan et al., 2012). Webb, Pearman, and Leuning (WPL) correction
132 was not applied here(Webb et al., 2007) because the instrument room was in a state of constant
133 temperature and pressure that converted the real-time concentration into a dry volume mixing ratio,
134 and the longer pipeline of the closed-path system avoided the influence of temperature fluctuations.
135 The limitations of eddy covariance systems can lead to frequency loss in flux observations. Factors
136 such as a limited average period and linear detrending can cause low-frequency loss, whereas
137 instrument separation, path averaging, insufficient high-frequency responses, and pipeline
138 attenuation can cause high-frequency loss. The method proposed by Moncrieff et al., (1996) was
139 employed for frequency response correction. After the above correction of the flux data, in this paper,
140 the 0-1-2 quality labeling scheme proposed by Mauder and Foken(Mauder et al., 2004) was adopted
141 for data quality control purposes. Notably, a value of 0 represents data with the best quality, a value
142 of 1 represents data with good quality, and a value of 2 represents data with poor quality. In this
143 study, flux data marked as 2 were excluded from the subsequent analysis. In addition, the flux source
144 area was evaluated via the method of Kljun et al., (2004) (Text. S1), and the flux source area covered
145 most of the urban area of Beijing and reflected the average emission characteristics of urban Beijing
146 (Figure S2).

147 **2.3 Spectral analysis**

148 High-frequency signal loss can occur in closed-path systems. To determine the response
149 capability of the closed-path system to high-frequency turbulence signals, we analyzed the observed
150 gas exchange signals through the turbulence power spectrum. The selected time ranges from 12:00
151 to 16:00 every day during the observation period, with a total of 8 and a half hours of data. The data
152 were integrated and averaged, and the data curve was then compared with the ideal slope in the
153 inertia subarea (Figure S3). $Co(wT)$ followed the theoretical $f_n^{-4/3}$ (where f_n denotes the normalized
154 frequency) in the inertial subregion. In contrast, the slopes of $Co(wCO_2)$ and $Co(wCH_4)$ were
155 slightly greater than $-4/3$, indicating that there was high-frequency loss in the flux observations of
156 the closed-loop system(Kaimal et al., 1972). Through high-frequency correction, the calculation
157 results indicated that the CO_2 and CH_4 fluxes were 7.73 % and 6.85 % greater, respectively, than
158 those before correction.

159 **2.4 Mobile CH_4 and CO_2 observations**

160 Vehicle-based experiments were conducted in the urban area of Beijing in the winter of 2023
161 and the summer of 2024, and the specific deployment of the mobile observation station is shown in
162 Figure S1. Notably, the car was equipped with a CO_2/CH_4 spectrometer (Los Gatos Research, Inc.,
163 USA), a laptop for data viewing, and a mobile power supply (Figure S4). Zero-point calibration of
164 the instrument was performed once pure nitrogen was used before the mobile experiment began.
165 Standard gases of methane and carbon dioxide were introduced to calibrate the instrument
166 simultaneously, and we found that the concentration of the instrument matched well with the
167 standard gas. Since we focused more on the enhancement in concentration rather than itself, we did
168 not calibrate it again afterward. The sampling port was located approximately 20 cm from the roof,
169 and ambient air was collected through a PTFE tube with a length of 2 m and an inner diameter of 3
170 mm. Before the particulate matter entered the instrument, it was removed using a filter head. The
171 IMET sounding instrument (International Met Systems, USA) is installed on the roof, with a
172 sampling frequency that is consistent with that of the other instruments, i.e., 1 s, real-time
173 concentration information of different latitudes and longitudes is obtained at a resolution of seconds
174 through the corresponding time between the GPS and the instrument; for example, if the GPS
175 sampling time delay is 3 s, the latitude and longitude coordinates are reassigned to the CH_4 reading

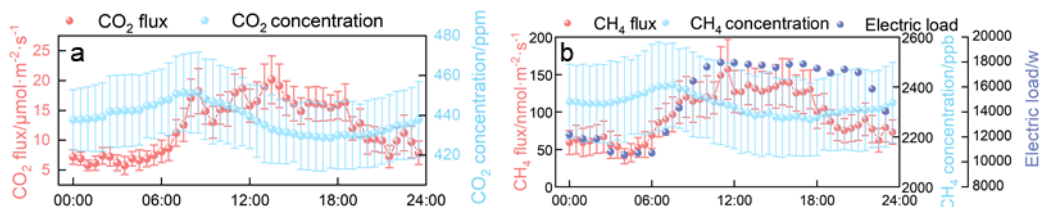
176 observed three seconds prior. Our observation sites include petrochemical plants located in
177 southwestern Beijing, natural gas storage tanks and landfills in the northeastern part, and power
178 plants with the highest natural gas usage in the southeastern part.

179 **3. RESULTS**

180 **3.1 Diurnal variation in the flux**

181 A positive or negative flux reflects the vertical exchange direction of trace gases in the urban
182 canopy, which is positive upward and negative downward. (The uncertainty analysis is described in
183 the Text. S2 and Figure S5, respectively) Overall, both CO₂ and CH₄ fluxes are positive on a daily
184 scale, indicating that cities are the source of both gases. The diurnal CO₂ flux ranged from 6.05 to
185 19.66 $\mu\text{mol}\cdot\text{m}^{-2}\cdot\text{s}^{-1}$ with an average of $12.21 \pm 1.75 \mu\text{mol}\cdot\text{m}^{-2}\cdot\text{s}^{-1}$ (Figure 1a), which was generally
186 lower than the summer observations by Cheng et al., (2018) and Liu et al., (2012) at 200 m and 140
187 m at this tower, respectively (Table S1), a smaller deviation suggests that CO₂ may be dominated by
188 a more stable source than before. We also obtained observation results at 140 m in summer from
189 2009–2017 (Liu et al., 2020). The flux in 2022 significantly decreased compared with previous
190 levels (Figure S6), which reflects the transformation of Beijing's energy structure. The coal-to-gas
191 policy implemented by Beijing these years led to a gradual decrease in the proportion of coal in
192 primary energy consumption, with a steady increase in the proportion of natural gas in total
193 consumption (Figure S7), the use of natural gas results in much less coal CO₂ than coal, generating
194 the same amount of heat; moreover, Beijing has increased the amount of electricity flow from other
195 provinces in recent years (Figure S7), which has further driven a decrease in the annual average
196 concentration of PM_{2.5}, dropping to 30.5 $\mu\text{g}\cdot\text{m}^{-3}$ by 2024. In fact, previous studies have reported a
197 high correlation between PM_{2.5} and CO₂ fluxes. For example, Donato et al., (2019) found that the
198 seasonal and daily variations in the particle number flux in southern Italian suburbs are largely
199 determined by both transportation activities and household heating. Liu et al., (2020) confirmed that
200 the CO₂ flux can explain 64 % of the interannual variation in the PM_{2.5} concentration by fitting the
201 correlation between the annual average PM_{2.5} and CO₂ fluxes in Beijing from 2009 to 2017.
202 Therefore, controlling CO₂ emissions can also greatly control the concentration level of PM_{2.5},
203 thereby achieving the dual effects of mitigating climate change and improving air quality. In terms
204 of its diurnal variation, it did not follow a typical bimodal pattern but rather remained high after

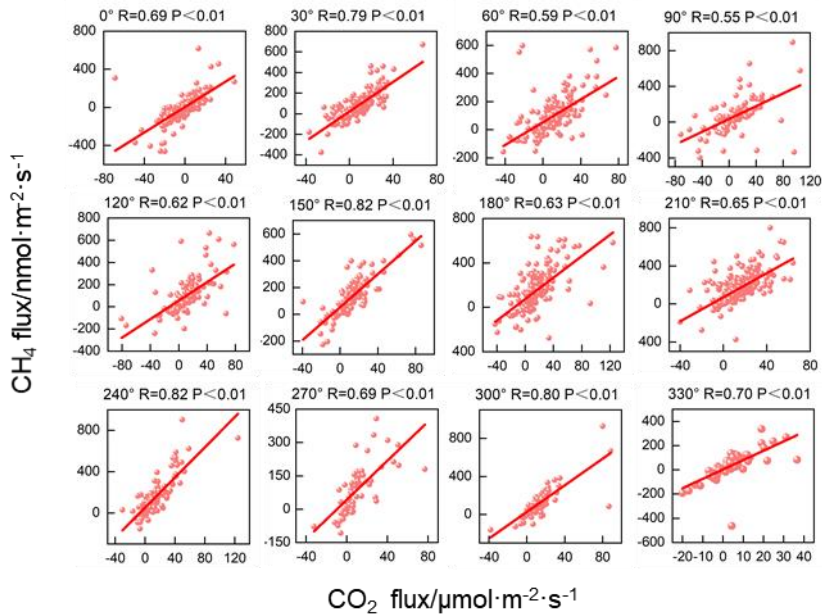
205 reaching the first peak at 8:00, with a lower level at night, reflecting high anthropogenic carbon
 206 emissions during the day, such as those resulting from transportation and energy generation
 207 activities. The diurnal pattern of the CH_4 flux was similar to the observation results of Giolo et al.,
 208 (2012) and Helfer et al., (2016) (Figure 1b), reflecting an increase in emissions during the day. The
 209 CH_4 flux began to increase gradually from 04:00 to around 08:30, and then remained stable until
 210 after 10:30, when it began to rise rapidly again, reaching its daily peak of approximately 157.1 nmol
 211 $\text{m}^{-2} \text{ s}^{-1}$ around 11:30. After 17:30, it slowly declined. Its diurnal variation pattern showed some
 212 differences compared to CO_2 flux, which increased beginning at 03:30 to around 08:30 similar to
 213 CH_4 flux. However, the peak for CO_2 flux occurred around 13:30, then slowly decreased and
 214 decreased rapidly after 18:30. Assuming that the average CH_4 flux at midnight (00:00 to 06:00) can
 215 be employed as the baseline for nighttime emissions, it accounted for 58 % of the daily average flux.
 216 The CH_4 flux demonstrated a pronounced diurnal pattern, indicating a significant daily variation in
 217 the background source in the source area.



218 Figure 1 Daily variations in the CO_2 and CH_4 concentrations, fluxes, and electricity loads

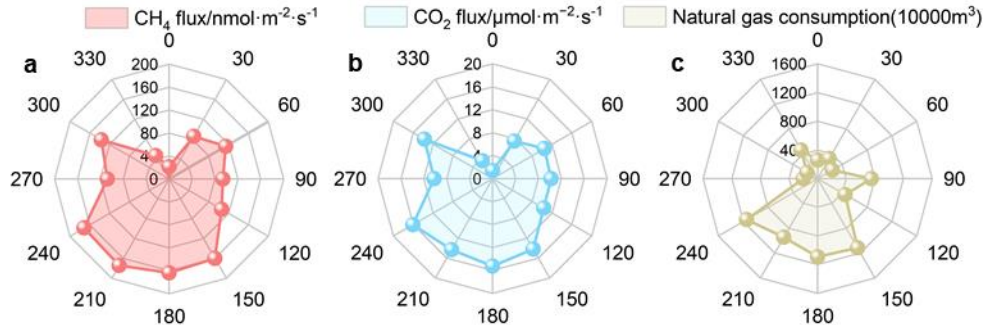
219 3.2 Homology between CO_2 and CH_4

220 The CO_2 and CH_4 fluxes showed a significant correlation along all directions (Figure 2), with
 221 correlation coefficients greater than that at the center of Loz, Poland (0.50)(Pawlak et al., 2016), but
 222 the low correlation between the CO_2 and CH_4 fluxes and the temperature excludes the conclusion
 223 that biological sources dominate their emissions (Figure S8). Therefore, CO_2 and CH_4 share the
 224 same anthropogenic sources within the source area. This homology is also reflected in their spatial
 225 distributions, with high fluxes distributed mainly south of the tower, which is more densely
 226 populated and encompasses complex industrial structures, and much lower fluxes in the northern
 227 forest and park areas (Figure 3a, b). The correlation between the spatial distributions of the CO_2 and
 228 CH_4 fluxes reached 0.98, demonstrating the common impact of similar anthropogenic sources on
 229 their emissions. The linear fitting results at 150° and 240° indicated the highest correlation
 230 coefficient (0.82) along all directions (Figure 2), further supporting this viewpoint.



232

233 Figure 2 Linear fitting results for the 30-minute CH₄ and CO₂ fluxes in the 12 directions



234

235 Figure 3 Mean CH₄ and CO₂ concentrations, fluxes and natural gas consumption in the 12
236 directions

237 4. DISCUSSION

238 4.1 Driver of the homology between CO₂ and CH₄

239 After the introduction of natural gas in 1985, the proportion of natural gas in the fossil fuel
240 industry of Beijing increased annually, especially when coal was replaced with natural gas and
241 electricity in 2014 and 2018, respectively, and natural gas became the most consumed fossil fuel
242 (Figure 6a). According to the 2022 Beijing Statistical Yearbook
243 (<https://nj.tjj.beijing.gov.cn/nj/main/2023-tnj/zk/e/indexch.htm>), natural gas is used mainly for
244 thermal power generation and heating (accounting for 69 %). Owing to the low proportion of heating
245 in summer, natural gas in Beijing is mostly used for thermal power generation in summer. Owing to
246 the difficulty in obtaining hourly electricity generation data, we obtained a daily variation curve of

247 the electricity load in Beijing based on the statistical data (power plants usually calculate the
248 required electricity generation based on the electricity load) (<https://www.gov.cn/xinwen/2019-12/30/5465088/files/e3682ce168c8427b886a43a790d66c2c.pdf>) (Figure 1b). The daily variation in
249 the electricity load is highly consistent with that in the CH₄ flux, with the maximum CH₄ flux
250 occurring at 11:00 pm during the peak electricity consumption period. After 16:00 pm, the electricity
251 load and CH₄ flux decrease synchronously. Thus, the daily variation in the CH₄ flux is driven by
252 natural gas consumption. We gridded the natural gas consumption data (Figure S9) and calculated
253 the mean natural gas consumption along all directions within the flux source area (Figure 3c).
254 Notably, a high consistency between the spatial distributions of the CO₂ and CH₄ fluxes and natural
255 gas consumption was found, which reflects that after the adjustment of the energy structure in
256 Beijing, natural gas became the main source of CO₂ and CH₄. Considering the high photosynthetic
257 absorption of CO₂ by plants in summer, this conclusion also applies to the other seasons, which
258 supports the hypothesis that natural gas is the main source of winter CO₂ emissions in Beijing, as
259 determined based on the isotope tracing method(Wang et al., 2022; Wang et al., 2022).
260

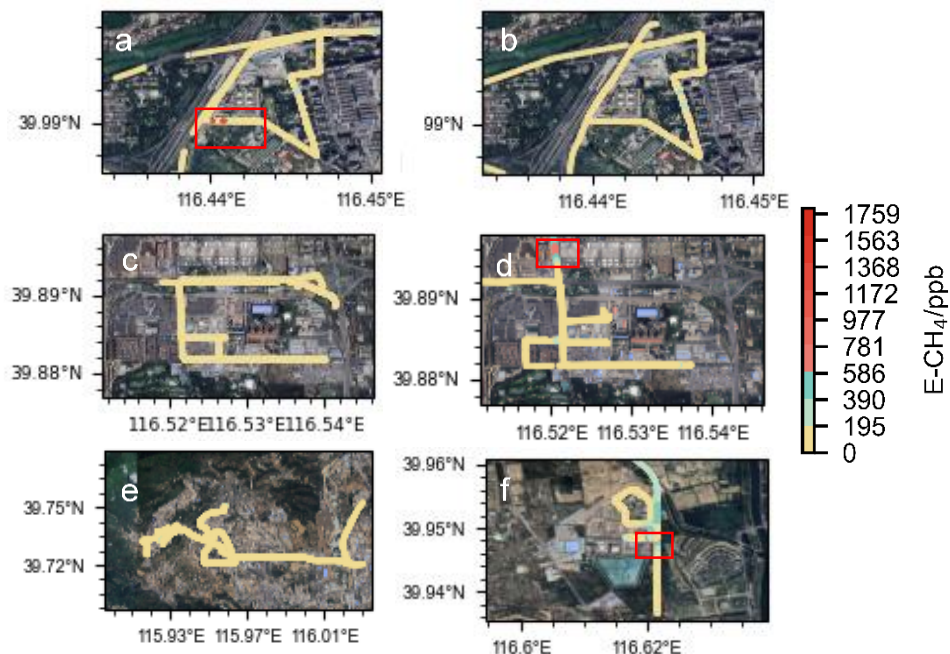
261 To verify this conclusion and identify the primary phases of natural gas leakage, we conducted
262 mobile observations during winter and summer around large petrochemical plants, gas storage tanks,
263 and power plants in Beijing. Given real-time variations in gas concentrations influenced by
264 meteorological conditions and pollution transport, it was essential to determine background
265 concentrations at each time point. The current mainstream approach for determining background
266 values involves calculating the 5th or 10th percentile within a sliding window of 5 minutes (± 2.5
267 min) or 10 minutes (± 5 min) centered on the target timestamp (Pu et al., 2023, Well et al., 2018;
268 Well et al., 2019). We compared and evaluated the results applying different combinations of time
269 windows or percentile following the method of Schiferl et al., (2025). (Text. S3). The 10-min time
270 window with 5th percentile was used here to calculate the background value. The enhancement
271 concentration can be defined as the difference between the observed value and the background value
272 at the corresponding time. There was significant CH₄ leakage around the gas storage tanks and
273 power plants in both winter and summer. Notably, the observed CH₄ hotspots were located in the
274 downzone of potential leakage sources; therefore, we attribute the high CH₄ concentration to the
275 emissions of these potential natural gas leakage sources. In winter, hotspots with concentrations

higher than the background value of 1759 ppb appeared around the gas storage tank (Figure 4a), corresponding to an enhancement concentration of CH₄ (E-CH₄) and enhancement concentration of CO₂ (E-CO₂) fingerprint line with a slope of 0.11 (Figure 5a). In addition, the enhancement concentration fingerprint slopes of the other hotspot zones were 0.06 and 0.07, respectively, indicating varying degrees of leakage around the gas storage tank(Sun et al., 2019).The enhancement concentration fingerprint in summer also revealed leakage related to gas storage equipment (Figure 4b), with a slope of 0.04, analogous to that of 0.06 in winter. Similar to gas storage tanks, natural gas leakage hotspots have been observed in various equipment in power plants. For example, fingerprints with a slope of 0.005 (Figure 5d) in summer reflected leakage related to combustion devices or pipeline in power plants(Lamb et al., 1995), whereas fingerprints with a slope of 0.015, 0.02 or 0.05 reflected leakage related to storage facilities (Figure 5c,d)(Hurry et al., 2016). We also discovered natural gas leakage near the petrochemical plant (Figure 4e), the line with a slope of 0.02 was related to the gas storage equipment, and the line with a slope of 0.005 was relevant to the natural gas combustion equipment. As important sources of methane, landfills have received widespread attention, so we also conducted mobile observations near a large landfill outside the Fifth Ring Road in Beijing, which was a hotspot exhibiting a level exceeding the minimum concentration of 1375 ppb (Figure 4f). The concentration fingerprints were relatively disordered and significantly differed from those of CH₄ emissions dominated by natural gas (Figure 5f), indicating that waste disposal processes are relatively complex and cannot be ignored in cities(Cusworth et al., 2024).

Converting observed concentration increments into emission rates is a simple means of quantifying natural gas leakage, which is subject to atmospheric conditions and potential leak source locations. Weller et al., (2018; 2019) developed a model based on the relationship between the enhancement concentration and emission rate. The specific formula is shown in Text S4. The model assumes that CH₄ enhancement is the best predictor of the leakage emission rate and that a greater leakage emission rate corresponds to greater CH₄ enhancement. The method sets a minimum threshold for the observed CH₄ concentration, which is 110 % of the background value, to filter out concentration changes caused by measurement. Moreover, when multiple detections are conducted for the same leakage source, it is necessary to average the CH₄ enhancement values and then

305 substitute them into the above formula. We estimated the natural gas leakage emission rates from
 306 different leakage sources with this method, and the confidence interval (CI) based on the Bootstrap
 307 method was used to estimate the uncertainty of the leakage rate. The natural gas leakage rate from
 308 the gas storage tank and power plant in winter were 7.4 ± 0.1 g/min and 0.6 ± 0.03 g/min,
 309 respectively, and the natural gas leakage rate from the gas storage tank and power plant in summer
 310 were 1.2 ± 0.04 g/min and 2.1 ± 0.07 g/min, respectively. The natural gas leakage rate near the
 311 petrochemical plant was 0.6 ± 0.04 g/min, which was lower than the results of Ars et al., (2020) on
 312 the leakage rates of Toronto's natural gas distribution network (3.52–10.56 g/min), but they noted
 313 that Well's method underestimated the leakage rate because it ignored smaller concentration
 314 enhancements. A significant uncertainty in this method lies in the distance between the leakage point
 315 and the vehicle; unfortunately, determining the distance between the two points in practical
 316 operation is difficult, which may confound the estimation of methane leakage. Therefore, sufficient
 317 mobile experiments should be conducted in subsequent work to accurately calculate natural gas
 318 leakage in Beijing.

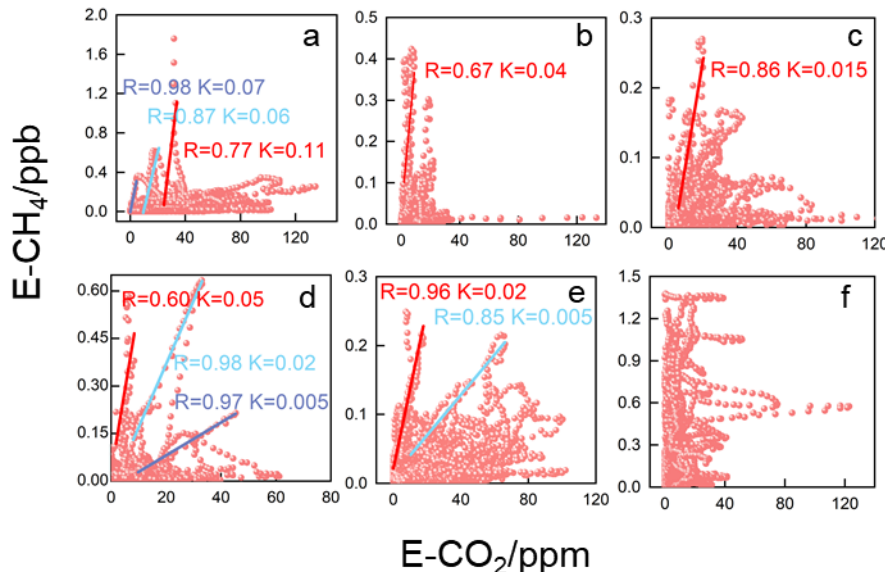
319



320

321 Figure 4 CH₄ enhancement concentration distribution map based on vehicle observations (a, c
 322 show storage tanks and thermal power plants in winter; b, d show storage tanks and thermal power
 323 plants in summer; e shows petrochemical plants; f shows waste disposal station; and the red box

324 represents high leakage value, the map is from Google earth: <https://earth.google.com/>)



325

326 Figure 5 Fitting of the CO₂ and CH₄ concentration enhancement values (a, c show the fitting
327 results for the gas storage tanks and power plants in winter; b, d show the fitting results for the gas
328 storage tanks and power plants in summer; e shows the petrochemical plants; and f shows the
329 waste disposal stations. Different fitting lines represent various leakage sources.)

330 4.2 Climatic effects of natural gas (NG) losses and their impact on carbon neutrality

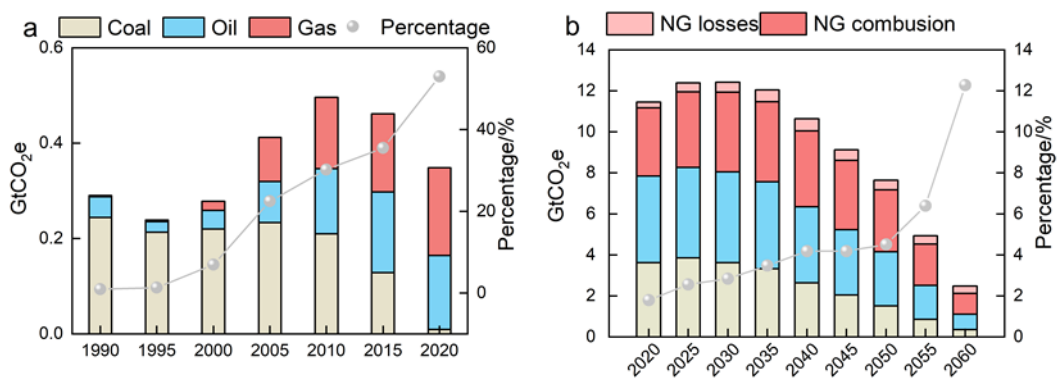
331 Based on the natural gas consumption and flux data for the flux source area, the estimated
332 upper limit of the natural gas leakage rate in Beijing reached 1.12 % \pm 0.22 % (Text. S5), and the
333 lower limit of natural gas leakage in Beijing was estimated to be 0.82 % considering the emissions
334 from biogenic sources (Text. S6). If the CH₄ fluxes were attributable solely to pipeline leakage
335 processes, the CH₄ fluxes should remain relatively stable throughout the day without significant
336 diurnal variations, given the constant pressure in urban pipeline pressures. However in our
337 observations, the CH₄ fluxes exhibited pronounced diurnal patterns and their spatial distribution
338 positively correlated with natural gas consumption. This indicates that CH₄ emissions in Beijing
339 originate predominantly from consumption-oriented leakage processes. Consequently, as natural
340 gas consumption surges during winter heating periods, CH₄ emissions from these processes (e.g.,
341 fugitive emissions from electrical devices) also increase. As a result, the ratio of emissions to
342 consumption (leakage rate) remains relatively stable. Thus, the CH₄ leakage rate measured in
343 summer is representative of year-round leakage rate of natural gas.

344 Our measured leakage rate was lower than the value of 2.07 % calculated based on the purchase
345 and sales statistics and the statistical mean value of 1.1 %–1.65 % reported by the American
346 Petroleum Institute (<https://www.api.org/>). Nevertheless, the contributions of CH₄ to climate
347 warming are 8.37 % and 23.17 % of those of CO₂ at the 100- and 20-year scales, respectively,
348 according to the determined CO₂ and CH₄ fluxes and the GWP of methane. With the arrival of the
349 winter heating season, climate forcing will further increase on a yearly scale. Assuming that the
350 natural gas consumption in Beijing during the heating season is 5 times greater than that during the
351 other seasons (according to Beijing Gas in 2019), that oil consumption does not significantly
352 fluctuate throughout the year and that both the CO₂ and CH₄ fluxes are positively correlated with
353 fossil fuel consumption and natural gas leakage, the climate forcing effect of natural gas leakage in
354 2022 was 11.47 % on a 100-year scale and could reach as high as 31.56 % on a 20-year scale.
355 However, when the same amount of heat is generated, the use of natural gas could yield CO₂
356 emission reductions of 50 % relative to coal and of only approximately 30 % relative to oil.
357 Therefore, the reduction in greenhouse gas emissions resulting from natural gas combustion
358 compared with that resulting from the combustion of other fossil fuels may be offset by the climate
359 forcing effect of CH₄ leakage in the short term, making it difficult for natural gas to become a
360 transitional energy source for energy transition.

361 To assess the impact of natural gas leakage on carbon peak and carbon neutrality bas
362 ed on our quantified leakage rate, scaling the Beijing-derived leakage rate to a national le
363 vel is needed. However, due to the absence of leakage rate data from other cities, we can
364 provide only a rough estimate based on available data as follows: according to the 14th
365 Five-Year Plan for National Urban Infrastructure Development (<https://www.gov.cn/zhengce/>
366 zhengceku/2022-07/31/5703690/files/d4ebd608827e41138701d06fe6133cdb.pdf), cities in Chin
367 a are divided into three categories—major cities (natural gas penetration rate \geq 85 %), med
368 ium cities (natural gas penetration rate \geq 75 %), and small cities (natural gas penetration ra
369 te \geq 60 %). The China Gas Development Report 2023 further supplements pipeline coverag
370 e progress(<https://www.emerinfo.cn/download/zgtrqfzbg2003001.pdf>), indicating that large citi
371 es and developed regions (e.g., Beijing, the Yangtze River Delta, the Pearl River Delta) a
372 ccounted for approximately 30 %–40 % of the national pipeline length in 2022, here set a

373 t 35 %. Small/medium cities constituted 60 %–70 % of the total pipeline length, here set
 374 at 65 %. A study based on Bayesian network modeling revealed that leakage probabilities
 375 in small/medium cities are 1.8 times higher than those in major cities (95% CI: 1.6–2.0)
 376 (Gao et al., 2024). Consequently, the national leakage rate was calculated as 1.7 % (95 %
 377 CI: 1.57 %–1.85 %)= $0.35 \times 1.12 \% + 0.65 \times 1.12 \% \times 1.8$ (95 % CI:1.6–2.0).

378 Then we adopted the results of the Global Climate Governance Strategy and China's Carbon
 379 Neutrality Path Outlook(Wang et al., 2021), which indicates that CO₂ emissions in China under the
 380 carbon neutrality scenario reach approximately 2.1 Gt. We calculated CH₄ leakage in the
 381 corresponding year based on the natural gas consumption level under the future scenario of the
 382 China Energy Outlook 2060 (SINOPEC 2021)(Economics-and-Development-Research-Institute,
 383 2021). All of the calculation results were converted CO₂ equivalents (CO₂e) according to the GWP
 384 on a 20-year scale (Figure 6b). After taking into account the natural gas leakage process, the CO₂e
 385 in China will still peak by 2030. However, the CO₂e resulting from natural gas leakage will reach
 386 0.37 Gt (95 % CI: 0.34 Gt–0.40 Gt) in 2060, compared to 0.26 Gt previously. This accounts for
 387 approximately 16.6 % (95 % CI: 15.4 %–17.9 %) of the total CO₂ emissions (excluding natural gas
 388 leakage) and 35.9 % (95 % CI: 33.2 %–38.8 %) of the total CO₂ emissions from natural gas
 389 combustion, which is comparable to the CO₂ emissions from coal combustion (0.35 Gt). Since
 390 natural carbon sinks do not show significant short-term fluctuations, the future increase in carbon
 391 sinks will mainly rely on carbon capture and storage (CCS) technology. Given the current estimated
 392 CO₂ capture rate of CCS technology (0.1 Gt/year, as estimated by the China Energy Outlook 2060
 393 (SINOPEC 2021)), the achievement of carbon neutrality in China will likely be delayed by nearly
 394 three to four years. Therefore, when determining future natural gas consumption levels, it is
 395 necessary to both consider the leakage effects of natural gas and utilize carbon modeling.



396

397 Figure 6 Terminal consumption of coal, oil, and natural gas and their proportions from 1990 to
398 2020(a) Since diesel-powered trucks are allowed only at night on the Fifth Ring Road and
399 kerosene, which is used mainly in aviation and is not included in the flux source area, oil mainly
400 comprises gasoline in this case), CO₂ equivalent from coal, oil and natural gas (losses and
401 combustion) in the future scenario (estimated by China Energy Outlook 2060 released by
402 SINOPEC in 2021), and CO₂ equivalent of natural gas leakage as a proportion of natural gas (NG)
403 combustion emissions(b)

404 **4.3 Policy implications**

405 Our observations revealed a strong correlation between CH₄ emissions and natural gas
406 consumption in terms of both their daily variations and spatial distributions, that is to say, the
407 terminal consumption process drive natural gas leakage in Beijing. Liu et al., (2023) established a
408 bottom-up emission inventory and reported that the terminal use process in Beijing accounts for 80 %
409 of the total methane emissions in the entire natural gas supply chain. Therefore, the Chinese
410 government may need to expand the detection of pipeline leakage to the entire natural gas industry
411 chain.

412 Notably, existing grid-based inventory products also exhibit significant uncertainty in terms of
413 methane sources. The extracted inventory originates from the Emissions Database for Global
414 Atmospheric Research (EDGAR) (<https://edgar.jrc.ec.europa.eu/EDGARv8.0>). Although the mean
415 methane flux (126.3 nmol·m⁻²·s⁻¹) within the source area is close to our results, the terminal use
416 process accounts for only approximately 13 % of the annual methane emissions, suggesting that
417 many potential urban methane sources could have been missed, which should be considered in
418 inventory refinement in the future.

419 In addition, minimizing the methane leakage rate could ensure the early realization of carbon
420 neutrality in China. Although methane emission control has been included in the agenda for the first
421 time in the Methane Emission Control Action Plan promulgated in 2023, which clearly highlights
422 the need to promote the application of leak detection and repair technology and to enhance the
423 comprehensive recovery and utilization of methane, methane leakage standards have not been
424 updated. Previous methane leakage standards focused only on controlling the amount of methane
425 leakage from a safe perspective, thereby ignoring the climate effects of natural gas leakage. China
426 must urgently develop a strict and detailed set of natural gas leakage standards.

427 **4.4 Limitations**

428 The flux discussed in this study is net flux, which means considering both positive flux and

429 negative flux simultaneously. It should be noted that for flux values close to zero (particularly the
430 negative values observed at night), we have retained all the data points without employing a filtering
431 method based on the statistics of instrument white noise. Whereas a more rigorous approach would
432 be to model these fluxes fluctuating around zero as white noise and establish a statistical significance
433 threshold based on this. Discarding all values within this threshold (including slightly positive and
434 slightly negative ones) could effectively reduce noise-induced bias, although at the cost of data
435 coverage. The development and application of such objective, instrument-physics-based filtering
436 criteria represent an important direction for future research to enhance the quality and reliability of
437 flux data, particularly under low-turbulence conditions.

438 For the source analysis of CO₂ and CH₄, we did not consider the impact of long-distance
439 transportation. However, this impact may not be completely ignored. For example, in the upwind
440 area of Beijing, Shanxi Province is a high-intensity area of anthropogenic pollutant emissions, where
441 the actual lifespan of local CO may be significantly shortened due to the influence of local OH
442 concentration. The CO₂ produced by CO there is not insignificant (Li et al., 2025), which may also
443 be one of the sources of local CO₂ in Beijing. Therefore, it is necessary to combine regional chemical
444 transport models to more accurately quantify the impact of local chemical coupling in future flux
445 research.

446 When quantifying CH₄ leakage from different natural gas facilities, we adopted a quantile
447 based deterministic method to separate background concentration from enhanced signals, and
448 mainly explored the sensitivity brought by algorithm parameter selection. However, this framework
449 has a fundamental limitation: it fails to incorporate the inherent observational uncertainty of
450 background concentration and on-site observed concentration into a unified probabilistic analysis.
451 The observation error of background value and enhanced signal are coupled (Lu et al., 2025; Zheng
452 et al., 2025), they will propagate together, and significantly affect the final uncertainty interval of
453 emission estimation. Our current sensitivity analysis can only be one step in such comprehensive
454 uncertainty quantification work (i.e. identifying sensitivity to parameter selection), and future work
455 should focus on: (1) systematically quantifying the instrument errors used in this study; (2)
456 integrating these prior uncertainties into the inversion process of emissions using probabilistic
457 frameworks such as Bayesian inference or error propagation models; (3) expanding the emission

458 estimation from a single 'best estimate' to a probability distribution that includes confidence
459 intervals.

460 Although we estimated the impact of natural gas leaks on China's carbon neutrality process,
461 the national-scale extrapolation of the natural gas leakage rate conducted in this study carried
462 substantial uncertainty. Our approach, which relied on a simplified scaling method due to data
463 availability constraints, may fail to account for strong regional heterogeneities in natural gas
464 consumption patterns and infrastructure conditions. As highlighted by recent literatures (Qin et al.,
465 2023; Hu et al., 2024), such scaling methods can systematically miss substantial emission sources
466 in specific regions (e.g., industrial hubs like Shanxi Province). Therefore, our national estimate
467 should be interpreted as a rough attempt.

468 **5. Conclusions and outlooks**

469 This study utilized the eddy covariance method to measure CO₂ and CH₄ fluxes at 220-m height
470 in urban Beijing, providing critical insights into surface-atmosphere exchanges of greenhouse gases
471 in the region. First, urban areas unequivocally act as net sources of both CO₂ and CH₄. The daily
472 mean fluxes were $12.21 \pm 1.75 \text{ } \mu\text{mol} \cdot \text{m}^{-2} \cdot \text{s}^{-1}$ for CO₂ and $95.54 \pm 18.92 \text{ } \text{nmol} \cdot \text{m}^{-2} \cdot \text{s}^{-1}$ for CH₄, with
473 daytime emissions significantly exceeding nighttime levels, highlighting the importance of
474 anthropogenic influences.

475 Although diurnal variation patterns differed slightly between CO₂ and CH₄ fluxes, their strong
476 correlation indicates shared dominant sources. Spatial distribution analysis revealed high
477 consistency between both fluxes and natural gas consumption patterns, confirming natural gas as a
478 common source. With Beijing's energy restructuring, natural gas has become the dominated
479 terminal energy consumption. Its combustion releases substantial CO₂, while leakage processes emit
480 CH₄, as validated by mobile observations detecting CH₄ fugitive emissions during production,
481 storage and use stages. Although biogenic sources could contribute to CH₄ emissions, they account
482 for at most 27 % of total CH₄ fluxes in the source area, ruling out the view that biological sources
483 dominate both emissions. Attributing all CH₄ emissions to natural gas usage, the upper leakage rate
484 of natural gas in Beijing was calculated as $1.12 \% \pm 0.22 \%$.

485 The CH₄ emissions from natural gas will exacerbate climate warming. Calculated flux results
486 showed that the contribution of CH₄ to climate warming on a century and 20-year scale can reach

487 as high as 8.37 % and 23.17 % of CO₂, respectively. On the basis of predicted energy report and
488 calculated leakage rate, it is roughly predicted that natural gas leakage will delay China's realization
489 of carbon neutrality, which necessitates urgent attention to mitigate associated climate effects.
490 Future work should prioritize the development of more granular, bottom-up inventories based on
491 province-level activity data and infrastructure surveys to achieve a more accurate and robust
492 assessment of China's overall natural gas leakage.

493 **SUPPORTING INFORMATION**

494 Details about the Beijing Meteorological Tower, eddy observation system and navigation
495 observation station, daily summer variation in CO₂ flux from 2009 to 2017, total consumption,
496 electricity inflow and the proportion of natural gas in total energy consumption from 2013-2022,
497 spatial distribution of CO₂ and CH₄ fluxes with wind speed and direction, grid distribution of natural
498 gas consumption in Beijing, calculation methods of the flux source area and natural gas leakage rate,
499 uncertainty analysis of flux calculation, estimation of non-natural gas sources

500 **ACKNOWLEDGMENTS**

501 This work was supported by the National Key R&D Program of China (2023YFC3706103), the
502 Strategic Priority Research Program of the Chinese Academy of Sciences (XDB0760200), the
503 Beijing Municipal Natural Science Foundation (No. 8222075), the Youth Cross Team Scientific
504 Research Project of the Chinese Academy of Sciences (No. JCTD-2021-10) and the S&T Program
505 of Hebei (22373903D).

506 **DATA AVAILABILITY**

507 All the data generated or analyzed in this study are included in the published article and are available
508 from the authors upon reasonable request.

509 **COMPETING INTERESTS**

510 The authors declare that they have no competing interests.

511 **REFERENCES**

512 Ars, S., Vogel, F., Arrowsmith, C., Heerah, S., Knuckey, E., Lavoie, J., Lee, C., Pak, N. M., Phillips,
513 J. L., and Wunch, D.: Investigation of the Spatial Distribution of Methane Sources in the
514 Greater Toronto Area Using Mobile Gas Monitoring Systems, Environ. Sci. Technol., 54,
515 15671-15679, <http://doi.org/10.1021/acs.est.0c05386>, 2020.
516 Barlow, J. F.: Progress in observing and modelling the urban boundary layer, Urban Climate, 10,
517 216-240, <http://doi.org/10.1016/j.uclim.2014.03.011>, 2014.

518 Chen, Z., Jacob, D. J., Nesser, H., Sulprizio, M. P., Lorente, A., Varon, D. J., Lu, X., Shen, L., Qu,
519 Z., Penn, E., and Yu, X.: Methane emissions from China: a high-resolution inversion of
520 TROPOMI satellite observations, *Atmos. Chem. Phys.*, 22, 10809-10826,
521 <http://doi.org/10.5194/acp-22-10809-2022>, 2022.

522 Cheng, X. L., Liu, X. M., Liu, Y. J., and Hu, F.: Characteristics of CO₂ concentration and flux in the
523 Beijing urban area, *J. Geophys. Res-Atmos.*, 123, 1785-1801,
524 <http://doi.org/10.1002/2017JD027409>, 2018.

525 Cusworth, D. H., Duren, R. M., Ayasse, A. K., Jiorle, R., Howell, K., Aubrey, A., Green, R. O.,
526 Eastwood, M. L., Chapman, J. W., Thorpe, A. K., Heckler, J., Asner, G. P., Smith, M. L., Thoma,
527 E., Krause, M. J., Heins, D., and Thorneloe, S.: Quantifying methane emissions from United
528 States landfills, *Science*, 383, 1499-1504, <http://doi.org/10.1126/science.adi7735>, 2024.

529 Cusworth, D. H., Jacob, D. J., Sheng, J.-X., Benmergui, J., Turner, A. J., Brandman, J., White, L.,
530 and Randles, C. A.: Detecting high-emitting methane sources in oil/gas fields using satellite
531 observations, *Atmos. Chem. Phys.*, 18, 16885-16896, <http://doi.org/10.5194/acp-18-16885-2018>, 2018.

533 Donateo, A., Conte, M., Grasso, F. M., and Contini, D.: Seasonal and diurnal behaviour of size
534 segregated particles fluxes in a suburban area, *Atmos. Environ.*, 219, 117052,
535 <http://doi.org/10.1016/j.atmosenv.2019.117052>, 2019.

536 Duren, R. M., Thorpe, A. K., Foster, K. T., Rafiq, T., Hopkins, F. M., Yadav, V., Bue, B. D.,
537 Thompson, D. R., Conley, S., Colombi, N. K., Frankenberg, C., McCubbin, I. B., Eastwood,
538 M. L., Falk, M., Herner, J. D., Croes, B. E., Green, R. O., and Miller, C. E.: California's methane
539 super-emitters, *Nature*, 575, 180-184, <http://doi.org/10.1038/s41586-019-1720-3>, 2019.

540 Economics-and-Development-Research-Institute: World and China Energy Outlook 2060,
541 <https://www.docin.com/p-2955292161.html>, 2021.

542 Environmental-Protection-Agency: Understanding global warming potentials,
543 <https://www.epa.gov/ghgemissions/understandingglobal-warming-potentials>, last accessed: 22
544 Oct. 2024.

545 Fan, S. M., Wofsy, S. C., Bakwin, P. S., Jacob, D. J., and Fitzjarrald, D. R.: Atmosphere–biosphere
546 exchange of CO₂ and O₃ in the central Amazon Forest, *JGR: Atmospheres*, 95, 16851-16864,
547 <http://doi.org/10.1029/JD095iD10p16851>, 2012.

548 Frankenberg, C., Thorpe, A. K., Thompson, D. R., Hulley, G., Kort, E. A., Vance, N., Borchardt, J.,
549 Krings, T., Gerilowski, K., Sweeney, C., Conley, S., Bue, B. D., Aubrey, A. D., Hook, S., and
550 Green, R. O.: Airborne methane remote measurements reveal heavy-tail flux distribution in
551 Four Corners region, *Proc. Natl. Acad. Sci. U. S. A.*, 113, 9734-9739,
552 <http://doi.org/10.1073/pnas.1605617113>, 2016.

553 Gao, S., Tian, W., and Wang, C.: A method, system, equipment, and medium for determining
554 methane leakage in a natural gas pipeline network: 202410249186, in Chinese, 2024.

555 Gioli, B., Toscano, P., Lugato, E., Matese, A., Miglietta, F., Zaldei, A., and Vaccari, F. P.: Methane
556 and carbon dioxide fluxes and source partitioning in urban areas: the case study of Florence,
557 Italy, *Environ Pollut*, 164, 125-131, <http://doi.org/10.1016/j.envpol.2012.01.019>, 2012.

558 Helfter, C., Tremper, A. H., Haliotis, C. H., Kotthaus, S., Bjorkegren, A., Grimmond, C. S. B., Barlow,
559 J. F., and Nemitz, E.: Spatial and temporal variability of urban fluxes of methane, carbon
560 monoxide and carbon dioxide above London, UK, *Atmos. Chem. Phys.*, 16, 10543-10557,
561 <http://doi.org/10.5194/acp-16-10543-2016>, 2016.

562 Hu, W., Qin, K., Lu, F., Li, D., and Cohen, J. B.: Merging TROPOMI and eddy covariance
563 observations to quantify 5-years of daily CH₄ emissions over coal-mine dominated region, *Int.*
564 *J. Coal Sci. Technol.*, 11, 56, <https://doi.org/10.1007/s40789-024-00700-1>, 2024.

565 Hurry, J., Risk, D., Lavoie, M., Brooks, B.-G., Phillips, C. L., and Göckede, M.: Atmospheric
566 monitoring and detection of fugitive emissions for Enhanced Oil Recovery, *Int. J. Greenh. Gas*
567 *Con.*, 45, 1-8, <http://doi.org/10.1016/j.ijggc.2015.11.031>, 2016.

568 Kaimal, J. C., and Finnigan, J. J.: Atmospheric boundary layer flows: their structure and
569 measurement. New York: Oxford University Press, 1994.

570 Kaimal, J. C., Wyngaard, J. C., Izumi, Y., and Coté, O. R.: Spectral characteristics of surface-layer
571 turbulence, *Quart. J. R. Met. Soc.*, 98, 563-589, <http://doi.org/10.1002/qj.49709841707>, 1972.

572 Kemfert, C., Präger, F., Braunger, I., Hoffart, F. M., and Brauers, H.: The expansion of natural gas
573 infrastructure puts energy transitions at risk, *Nature Energy*, 7, 582-587,
574 <http://doi.org/10.1038/s41560-022-01060-3>, 2022.

575 Kljun, N., Calanca, P., Rotach, M. W., and Schmid, H. P.: A Simple Parameterisation for Flux
576 Footprint Predictions, *Boundary-Layer Meteorology*, 112, 503-523,
577 <http://doi.org/10.1023/b:Boun.0000030653.71031.96>, 2004.

578 Lamb, B. K., McManus, J. B., Shorter, J. H., Kolb, C. E., Mosher, B., Harriss, R. C., Allwine, E.,
579 Blaha, D., Howard, T., Guenther, A., Lott, R. A., Siverson, R., Westburg, H., and Zimmerman,
580 P.: Development of atmospheric tracer methods to measure methane emissions from natural
581 gas facilities and urban areas, *Environ. Sci. Technol.*, 29, 1468-1479,
582 <http://doi.org/10.1021/es00006a007>, 1995.

583 Lee, X.: *Handbook of micrometeorology: A Guide for surface Flux Measurement and Analysis*.
584 New York: Klewer Academic Publishers, 2004.

585 Li, X., Cohen, J. B., Tiwari, P., Wu, L., Wang, S., He, Q., Yang, H., and Qin, K.: Space-based
586 inversion reveals underestimated carbon monoxide emissions over Shanxi, *Commun. Earth*
587 *Environ.*, 6, 357, <https://doi.org/10.1038/s43247-025-02301-5>, 2025.

588 Liu, H. Z., Feng, J. W., Järvi, L., and Vesala, T.: Four-year (2006–2009) eddy covariance
589 measurements of CO₂ flux over an urban area in Beijing, *Atmos. Chem. Phys.*, 12, 7881-7892,
590 <http://doi.org/10.5194/acp-12-7881-2012>, 2012.

591 Liu, S., Liu, K., Wang, K., Chen, X., and Wu, K.: Fossil-Fuel and Food Systems Equally Dominate
592 Anthropogenic Methane Emissions in China, *Environ. Sci. Technol.*, 57, 2495-2505,
593 <http://doi.org/10.1021/acs.est.2c07933>, 2023.

594 Liu, Z., Liu, Z., Song, T., Gao, W., Wang, Y., Wang, L., Hu, B., Xin, J., and Wang, Y.: Long-term
595 variation in CO₂ emissions with implications for the interannual trend in PM(2.5) over the last
596 decade in Beijing, China, *Environ. Pollut.*, 266, 115014,
597 <http://doi.org/10.1016/j.envpol.2020.115014>, 2020.

598 Lu, F., Qin, K., Cohen, J. B., He, Q., Tiwari, P., Hu, W., Ye, C., Shan, Y., Xu, Q., Wang, S., and Tu,
599 Q.: Surface-observation-constrained high-frequency coal mine methane emissions in Shanxi,
600 China, reveal more emissions than inventories, consistent with satellite inversion, *Atmos.*
601 *Chem. Phys.*, 25, 5837-5856, <https://doi.org/10.5194/acp-25-5837-2025>, 2025.

602 Mauder, M., and Foken, T.: Documentation and Instruction Manual of the Eddy Covariance
603 Software Package TK2, *Proc. R. Soc. Med.*, 26, 42-46, <http://doi.org/10.5281/zenodo.20349>,
604 2004.

605 Moncrieff, J. B., Malhi, Y., and Leuning, R.: The propagation of errors in long-term measurements
606 of land - atmosphere fluxes of carbon and water, *Global Change Biology*, 2, 231-240,
607 <http://doi.org/10.1111/j.1365-2486.1996.tb00075.x>, 1996.

608 Pawlak, W., and Fortuniak, K.: Eddy covariance measurements of the net turbulent methane flux in
609 the city centre – results of 2-year campaign in Łódź, Poland, *Atmos. Chem. Phys.*, 16, 8281-
610 8294, <http://doi.org/10.5194/acp-16-8281-2016>, 2016.

611 Pu, W., Sheng, J., Tian, P., Huang, M., Liu, X., Collett Jr, J.L., Li, Z., Zhao, X., He, D., Dong, F.:
612 On-road mobile mapping of spatial variations and source contributions of ammonia in Beijing,
613 China, *Sci. Total Environ.*, 864, 160869, 2023.

614 Qin, K., Hu, W., He, Q., Lu, F., and Cohen, J. B.: Individual coal mine methane emissions constrained
615 by eddy covariance measurements: low bias and missing sources, *Atmos. Chem. Phys.*, 24, 3009-
616 3028, <https://doi.org/10.5194/acp-24-3009-2024>, 2024.

617 Sargent, M. R., Floerchinger, C., McKain, K., Budney, J., Gottlieb, E. W., Hutyra, L. R., Rudek, J.,
618 and Wofsy, S. C.: Majority of US urban natural gas emissions unaccounted for in inventories,
619 *Proc. Natl. Acad. Sci. U. S. A.*, 118, e2105804118, <http://doi.org/10.1073/pnas.2105804118>,
620 2021.

621 Schiferl, L.D., Hallward-Driemeier, A., Zhao, Y., Toledo-Crow, R., and Commane, R.: Missing
622 wintertime methane emissions from New York City related to combustion, *EGUspHERE*, 2025,
623 1-28, <https://doi.org/10.5194/egusphere-2025-345>, 2025.

624 Seneviratne, S. I., Rogelj, J., Seferian, R., Wartenburger, R., Allen, M. R., Cain, M., Millar, R. J.,
625 Ebi, K. L., Ellis, N., Hoegh-Guldberg, O., Payne, A. J., Schleussner, C. F., Tschakert, P., and
626 Warren, R. F.: The many possible climates from the Paris Agreement's aim of 1.5 degrees C
627 warming, *Nature*, 558, 41-49, <http://doi.org/10.1038/s41586-018-0181-4>, 2018.

628 Shen, L., Jacob, D. J., Gautam, R., Omara, M., Scarpelli, T. R., Lorente, A., Zavala-Araiza, D., Lu,
629 X., Chen, Z., and Lin, J.: National quantifications of methane emissions from fuel exploitation
630 using high resolution inversions of satellite observations, *Nat. Commun.*, 14, 4948,
631 <http://doi.org/10.1038/s41467-023-40671-6>, 2023.

632 Sherwin, E. D., Rutherford, J. S., Zhang, Z., Chen, Y., Wetherley, E. B., Yakovlev, P. V., Berman, E.
633 S. F., Jones, B. B., Cusworth, D. H., Thorpe, A. K., Ayasse, A. K., Duren, R. M., and Brandt,
634 A. R.: US oil and gas system emissions from nearly one million aerial site measurements,
635 *Nature*, 627, 328-334, <http://doi.org/10.1038/s41586-024-07117-5>, 2024.

636 Sun, W., Deng, L., Wu, G., Wu, L., Han, P., Miao, Y., and Yao, B.: Atmospheric Monitoring of
637 Methane in Beijing Using a Mobile Observatory, *Atmosphere*, 10, 554,
638 <http://doi.org/10.3390/atmos10090554>, 2019.

639 Vickers, D., and Mahrt, L.: Quality Control and Flux Sampling Problems for Tower and Aircraft
640 Data, *J. Atmos. Oceanic Technol.*, 14, 512-526, [http://doi.org/10.1175/1520-0426\(1997\)014<0512:Qcafsp>2.0.Co;2](http://doi.org/10.1175/1520-0426(1997)014<0512:Qcafsp>2.0.Co;2), 1997.

642 Wang, P., Zhou, W., Xiong, X., Wu, S., Niu, Z., Cheng, P., Du, H., and Hou, Y.: Stable carbon
643 isotopic characteristics of fossil fuels in China, *Sci. Total. Environ.*, 805, 150240,
644 <http://doi.org/10.1016/j.scitotenv.2021.150240>, 2022.

645 Wang, P., Zhou, W., Xiong, X., Wu, S., Niu, Z., Yu, Y., Liu, J., Feng, T., Cheng, P., Du, H., Lu, X.,
646 Chen, N., and Hou, Y.: Source Attribution of Atmospheric CO₂ Using ¹⁴C and ¹³C as Tracers
647 in Two Chinese Megacities During Winter, *JGR: Atmospheres*, 127, e2022JD036504,
648 <http://doi.org/10.1029/2022jd036504>, 2022.

649 Wang, Y., Guo, C. H., Chen, X. J., Jia, L. Q., Guo, X. N., Chen, R. S., and Wang, H. D.: Global
650 climate governance strategies and prospects for China's carbon neutrality path. *Forecasting
651 And Prospects Research Report*, 2021.

652 Webb, E. K., Pearman, G. I., and Leuning, R.: Correction of flux measurements for density effects
653 due to heat and water vapour transfer, *Q. J. R. Meteorolog. Soc.*, 106, 85-100,
654 <http://doi.org/10.1002/qj.49710644707>, 2007.

655 Weller, Z. D., Roscioli, J. R., Daube, W. C., Lamb, B. K., Ferrara, T. W., Brewer, P. E., and von
656 Fischer, J. C.: Vehicle-Based Methane Surveys for Finding Natural Gas Leaks and Estimating
657 Their Size: Validation and Uncertainty, *Environ. Sci. Technol.*, 52, 11922-11930,
658 <http://doi.org/10.1021/acs.est.8b03135>, 2018.

659 Weller, Z. D., Yang, D. K., and von Fischer, J. C.: An open source algorithm to detect natural gas
660 leaks from mobile methane survey data, *PLoS One*, 14, e0212287,
661 <http://doi.org/10.1371/journal.pone.0212287>, 2019.

662 Wunch, D., Toon, G. C., Hedenius, J. K., Vizenor, N., Roehl, C. M., Saad, K. M., Blavier, J.-F. L.,
663 Blake, D. R., and Wennberg, P. O.: Quantifying the loss of processed natural gas within
664 California's South Coast Air Basin using long-term measurements of ethane and methane,
665 *Atmos. Chem. Phys.*, 16, 14091-14105, <http://doi.org/10.5194/acp-16-14091-2016>, 2016.

666 Zheng, B., Cohen, J. B., Lu, L., Hu, W., Tiwari, P., Lolli, S., Garzelli, A., Su, H., and Qin, K.: How
667 can we trust TROPOMI based Methane Emissions Estimation: Calculating Emissions over
668 Unidentified Source Regions, *EGUsphere* [preprint], <https://doi.org/10.5194/egusphere-2025-1446>, 2025.

670 Zöll, U., Brümmer, C., Schrader, F., Ammann, C., Ibrom, A., Flechard, C. R., Nelson, D. D.,
671 Zahniser, M., and Kutsch, W. L.: Surface–atmosphere exchange of ammonia over peatland
672 using QCL-based eddy-covariance measurements and inferential modeling, *Atmos. Chem.
673 Phys.*, 16, 11283-11299, <http://doi.org/10.5194/acp-16-11283-2016>, 2016.

674